Molecular Dynamics Simulation of a Brine Droplet under Electric Field: Distinct Behavior Shown by NaCl and $CaCl_2$

Wenhui Li [a], Hongbo Zeng [a, *], and Tian Tang [b, *]

[a] Department of Chemical and Materials Engineering, University of Alberta, Edmonton, AB T6G 1H9, Canada

[b] Department of Mechanical Engineering, University of Alberta, Edmonton, AB T6G 1H9, Canada

** Corresponding authors:*

E-mail: hongbo.zeng@ualberta.ca (H.Z.); Phone: +1-780-492-1044;

E-mail: tian.tang@ualberta.ca (T.T.); Phone: +1-780-492-5467.

Abstract

Electrostatic demulsification is a promising technique to disrupt petroleum emulsions. However, the presence of salts in the emulsion can influence the effectiveness of the electric field. In this work, we target an understudied area, namely the effect of salt ion type and concentration on the stability of brine droplets when exposed to an electric field. Molecular dynamics (MD) simulations are performed on a series of water-in-oil emulsion systems consisting of a water or brine droplet surrounded by an oil phase containing toluene and model asphaltene molecules (N-(1-hexylheptyl)-N'-(5-carboxylicpentyl) perylene-3,4,9,10-tetracarboxylic bisimide (C5Pe)). The brine droplet contains either NaCl or $CaCl_2$, with concentration varying from 0 to ~11 wt%. An external electric field is applied, which has a strength ranging from 0 to 1 V/nm. Our results show that as the electric field increases, the bare water droplet exhibits progressive deformation from the original spherical shape to an ellipsoid, a spindle, and finally a cylinder. When the brine droplets are exposed to a low electric field ($\leq$ 0.5 V/nm), they behave similarly to the bare water droplet. However, at high electric field ($\geq$ 0.75 V/nm), both NaCl and $CaCl_2$ brine droplets are stabilized in the bulk oil and maintain the spherical or ellipsoidal shape by ejecting salt ions towards the electrodes at high salt concentrations ($\geq$ 7.8 wt %), which induces a counter electric field that weakens the destabilization of the droplet by the applied field. At low salt concentrations ($\leq$ 4.5 wt %), brine droplets containing NaCl or $CaCl_2$ display different behaviors: the former tends to shift towards an electrode, whereas the latter stays in the bulk oil phase. The contrasting phenomena are the result of combined effects of brine droplet net charge and C5Pe adsorption on the droplet surface: a large net charge and low C5Pe adsorption tend to drive the droplet towards an electrode. This study provides useful insights into the important role of salt ions in electrostatic demulsification of petroleum emulsions.

Keywords: Electrostatic demulsification; NaCl; $CaCl_2$; Salt concentration; Droplet deformation; Molecular dynamics simulation

1. Introduction

Emulsions commonly exist in many industrial processes such as food processing, metal manufacturing, and petroleum production [1-4]. As a specific example, water-in-oil emulsion is routinely encountered in bitumen froth treatment of oil sands production, among other emulsions such as oil-in-water and more complex water-in-oil-in-water emulsions [1, 5]. The existence of emulsions in bitumen froth treatment can lead to corrosion and fouling issues, resulting in additional costs and environmental concerns [2, 6]. It is challenging to separate small dispersed water droplets from the oil phase, especially when the emulsions are stabilized by indigenous compounds in the crude oil, such as asphaltenes and resins [2, 6-9]. Electrostatic demulsification by applying an external electric field is a promising and cost-effective method [6, 10-11]. However, the omnipresence of salt ions in water [12-13] can influence the effectiveness of electrostatic demulsification. Salt ions can interact with emulsion stabilizers, and these two species can respond differently to the electric field [4, 14-18]. As a result, they might function synergistically or competitively in facilitating or inhibiting the deformation and coalescence of water droplets. It is therefore of great interest and significance to investigate the response mechanism of water-in-oil emulsion when exposed to an electric field and under the collective influence of salt ions and interface-active emulsion stabilizers.

The shape change and stability of an emulsion droplet caused by an electric field has been the subject of several previous studies [18]. Theoretically, it is hypothesized that under the electric field the droplet would undergo deformation, leading to rearrangement of the components inside the droplet [19-22]. The simplest theoretical model that describes the droplet deformation is the

Taylor's model [23]. In this model, it is assumed that the initial shape of the droplet is a sphere with radius r_d and after deformation it becomes a prolate spheroid with a long semi-axis of a and two equal short semi-axes of b. The deformed shape is predicted from the balance between electric stress ($\varepsilon_0 \varepsilon_m E^2$, where E is the electric field strength; ε_0 and ε_m are respectively the permittivity of vacuum and dielectric constant of the medium) and capillary stress (γ / r_d, with γ being the interfacial tension between the droplet and the medium), and given by the following equation

$$E\sqrt{\frac{2 r_d \varepsilon_0 \varepsilon_m}{\gamma}} = 2\left(\frac{b}{a}\right)^{\frac{4}{3}}\left[2 - \frac{b}{a} - \left(\frac{b}{a}\right)^3\right]^{\frac{1}{2}} f(e), \tag{1}$$

where $f(e) = \frac{1}{2} e^{-3} \ln\left(\frac{1+e}{1-e}\right) - e^{-2}$ and $e = \sqrt{1 - b^2/a^2}$. The left-hand side of Eq (1) can be recognized as $\sqrt{2Ca_e}$ where $Ca_e = \varepsilon_0 \varepsilon_m E^2 r_d / \gamma$ is the electric capillary number and measures the ratio between the electric and capillary stresses. γ can be determined via different approaches, both experimentally [24-26] and numerically [12, 27-28]. Taylor's model has been shown to be valid when Ca_e is within a critical threshold ($(Ca_e)_{critical}$) [18, 29-31] and consequently the droplet deformation is small. Later, a modified version of Taylor's model was proposed by Garton and Krasucki [31] by considering finite permittivity of the droplet. Ajayi also improved the Taylor's model by including higher-order corrections that address the issue of underestimated deformation by the original Taylor's model [32]. Abbasi et al. [29] measured the deformation of a castor oil droplet in silicone oil under electric field, and proposed a model to describe the transition from equilibrium deformation (when $Ca_e < (Ca_e)_{critical}$) to non-equilibrium deformation (when $Ca_e > (Ca_e)_{critical}$). Gong et al. [33] found that when subjected to a pulse electric field, a water droplet in oil exhibited vibrational motion in the form of periodic stretching and compression, which is potentially beneficial for the coalescence of emulsion droplets. The authors also developed a model to describe the vibration, which agreed well with experimental results. While these models provide simple predictions for the deformation of a pristine droplet, the presences of salt ions and surface-active compounds are not explicitly considered.

Experimentally, the development of high-speed imaging technologies has enabled direct monitoring of droplet deformation. Berg et al. [34] found that under an electric field the deformation of a water droplet in surfactant-free oil is consistent with the Taylor's model, while the deformation is reduced in an oil that contains surfactants. They attributed the reduced deformation to the increased stiffness of the water-oil interface caused by the adsorption of surfactants. Luo et al. [30] observed similar phenomena in a comparable set of experiments, but provided a different explanation. It was postulated that the droplet deformation caused increase of the interfacial area, which led to the decrease in surface coverage by the surfactants and subsequently the increase of interfacial tension. As a result, Ca_e decreased, hindering further deformation of the droplet. Ervik et al. [35] studied a water droplet immersed in an oil phase containing non-ionic surfactants and subjected to an electric field. The droplet was observed to be able to stretch slightly beyond the breakup limit in Taylor's prediction, due to the presence of surfactants [23]. In addition, at high surfactant concentrations a significant hysteresis was observed when the droplet underwent cyclic loading with increasing electric field strength. Besides droplet deformation, several works also reported droplet breakage and generation of small daughter droplets, when the applied electric field was sufficiently strong [19, 23, 29, 36-37]. Producing daughter droplets lowers the average droplet size, which adversely affects coalescence and phase separation. Therefore, the strength of the electric field should be appropriate so as to not introduce droplet breakage. It should be mentioned that none of the above experimental studies considered the presence of salt or the potential influence of ions on droplet deformation and stability.

Recently, molecular dynamics (MD) simulations have shed light in this area by providing atomistic insights into the coalescence and deformation of emulsion droplets. To reduce the computational cost, most of these simulations focused on the coalescence of multiply water (or brine) droplets in nitrogen gas phase [38-46], instead of in a continuous oil phase. There are a few exceptions [38, 47-48], where water-in-oil emulsion was investigated and the effects of surfactant, droplet size and net charge, and electric field (constant or pulsed) on the coalescence of emulsion droplets were explored. To our knowledge, MD study on the response of a single droplet to an external electric field has only been performed by Li et al. in their recent series of works[49-51]. The simulation systems in their studies include a NaCl brine droplet with salt concentration of 5.5 wt% in a continuous nitrogen gas phase [49], a NaCl brine droplet with salt concentration of 1.7 wt% in an oil phase (represented by a mixture of hexane, cycloheptane, and benzene) [50], and a NaCl brine droplet (salt concentration 0.7 wt%) surrounded by model naphthenic acids molecules immersed in n-hexane phase [51]. They found that the droplet deformation increased with the strength of the electric field. When the electric field strength exceeded a critical value, droplet breakup occurred and three breakup patterns were observed (from one end, from two ends, and from the center) [49-50], which was consistent with experimental observations at mesoscopic scales [29]. Naphthenic acids molecules were found to adsorb onto the middle portion of the droplet during its deformation and breakup, making the two ends exposed to the oil phase [51]. Salt ions were claimed to migrate with the electric field, which favored droplet breakup [49-51].

While the studies by Li et al. [49-51] are informative and valuable, in the present work we intend to fill two gaps that still exist. First, the previous studies [49-51] only considered NaCl as the salt. In reality, brine in petroleum emulsion contains many types of ions [52] which can respond differently to an external electric field. In particularly, experiments have shown the presence of a proper amount of Ca^{2+} could enhance oil recovery in low salinity water flooding [53-56], but the underlying mechanisms are unclear. In this work, brine droplets containing NaCl and $CaCl_2$ are compared to investigate the potential difference caused by Na^+ and Ca^{2+} ions. Second, the salt concentration in petroleum emulsion can be quite high (exceeding 10 wt%) [52]. The concentration considered by Li et al.[49-51] is relatively low, and only one concentration was considered in each study. Therefore, a systematic study on the salt concentration effect is still absent. To address this, a broad range of salt concentrations (from 0 to ~11 wt%) are simulated here. Together, we aim to provide a more comprehensive understanding on how the properties of salt ions influence the deformation and stability of a water-in-oil emulsion droplet subjected to an electric field.

2. Method

2.1. Simulated Systems

An example of the simulation systems is depicted in **Figure 1**. The left side of the simulation box contains a spherical water (or brine) droplet placed at the center of the oil phase, which serves as the model water-in-oil emulsion. The emulsion is sandwiched by two graphene sheets, which act as the anode and cathode. The graphene sheets also have the function of removing artifacts caused by periodic boundary conditions (PBCs) when the electric field is applied between them. In absence of the graphene sheets, under the electric field some charged particles would go out of the box from one end and re-enter it from the opposite end, and this would cause the electric field strength to deviate from the pre-set value [57]. To the right side of the model emulsion is a slab of vacuum, further screening the long-range interaction between the simulation box and its periodic images. The dimension of the model emulsion is $12\times12\times20$ nm^3, and the radius of the water (or brine) droplet is ~3 nm. The vacuum space is $12\times12\times40$ nm^3.

All the system details are listed in **Table 1**. The cation in brine is either Na^+ or Ca^{2+}, and the anion is Cl^-. Four different salt concentrations are considered (2.2, 4.5, 7.8, and 11.7 wt% for NaCl; 2.5, 4.5, 7.8, and 11.4 wt% for $CaCl_2$). Because the distribution of ions within the droplet is not uniform (especially near the brine-oil interface), their concentrations are calculated from the densities of salt ions and water in the bulk region of the brine droplet (1 nm $\leq r \leq$ 2 nm, with r being the distance from the center of mass (COM) of the brine droplet) during the sampling stage of the simulation under E = 0 V/nm. The base of the oil phase is modeled by toluene, which contains ~3.5 wt% of model asphaltene molecules represented by a polyaromatic compound N-(1-Hexylheptyl)-N-(5-carboxylicpentyl) perylene-3,4,9,10-tetracarboxylic bisimide (C5Pe, chemical formula shown in **Figure 1**) [58-59]. Such a composition of the oil phase has been widely used in experiments and simulations [2-3, 6, 60-61]. Electric field with various strengths (E = 0, 0.5, 0.75 and 1.0 V/nm) is applied along the z-direction, perpendicular to the electrodes. The electric field $\mathbf{E}$ is introduced by exerting a force, $\mathbf{F} = q\mathbf{E}$, on the charged particles, with q being the charge of the particle.

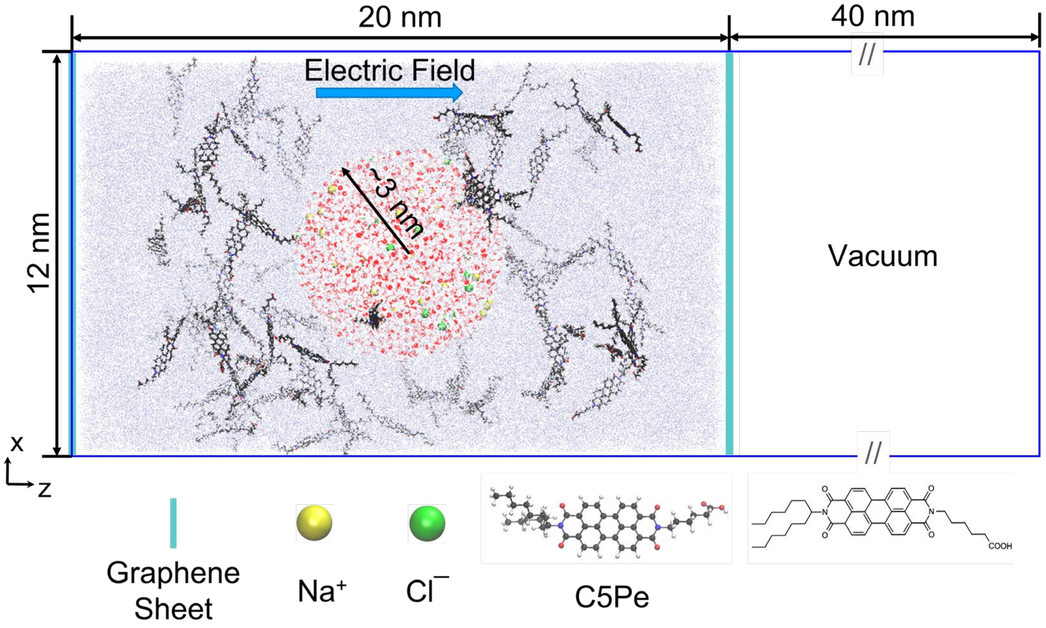

Figure 1 An example of the initial configuration of simulation systems (System S7_Na in **Table 1**). The base oil represented by gray points is toluene, and the sphere with radius of ~3 nm is the brine droplet which contains salt ions. The model asphaltene is represented by C5Pe, randomly dispersed in toluene. The black, red, blue, and white spheres in C5Pe are C, O, N, and H respectively, and its chemical formula is shown.

Table 1 Details of simulated systems. Numbers of C5Pe, water, and toluene molecules are 75, 4000, and 15500, respectively, in all the systems. For each system, electric fields with four different strengths (0, 0.5, 0.75 and 1.0 V/nm) are applied.

System	Numbers of cation (Na^+ or Ca^{2+}) & anion (Cl^-)	Salt Concentration (wt%)
S0	0 & 0	0
S2_Na	20 & 20	2.2
S2_Ca	10 & 20	2.5
S4_Na	40 & 40	4.5
S4_Ca	20 & 40	4.5
S7_Na	75 & 75	7.8
S7_Ca	38 & 76	7.8
S11_Na	120 & 120	11.7
S11_Ca	60 & 120	11.4

2.2. Simulation Details

All the systems are assembled by the PACKMOL package [62] and simulations are conducted using the GROMACS package (version 2021.2) [63-64]. For each system, energy minimization is first performed to ensure the maximum force on any atom is smaller than 1000 kJ/(mol·nm). Next, an annealing process in *NVT* ensemble is simulated for 60 ns, where the temperature for C5Pe is linearly increased from 300 to 500 K in the first 5 ns (0−5 ns), maintained at 500 K for 20 ns (5−25 ns), linearly reduced to 300 K in the next 25 ns (25−50 ns), and finally maintained at 300 K for 10 ns (50−60 ns). The temperature for the water (or brine) droplet and toluene is always kept at 300 K. This process facilitates the escape of heavy molecules from local potential energy wells. After the annealing simulation, an electric field is applied, and the simulation is run in *NVT* ensemble for 40 ns with the temperature maintained at 300 K. Of the 40 ns, the first 20 ns is used for equilibration (verified by the attainment of stable density profiles) and the last 20 ns for sampling and statistical analysis. The graphene sheets are frozen during the entire simulation. They are charge neutral and interact with the other components in the system via van der Waals interaction (Lennard-Jones potential as specified in the augmented OPLS-AA force field [65]).

The water model is TIP4P/2005 [66], which has been proven to produce accurate thermodynamic and transport properties under a broad range of temperatures and pressures [67-70]. The force field parameters for salt ions are from Madrid-2019 [71], which are proposed based on compatibility with the TIP4P/2005 water model and validated against experiments for a wide range of salt concentrations [ref]. It should be noted that Madrid-2019 is a scaled charge model, where chloride, sodium, and calcium ions carry charges of −0.85 e, +0.85 e and +1.70 e, respectively. However, for simplicity, we still refer to them as Cl^-, Na^+, and Ca^{2+}. It has been shown that the full charge ion models fail to accurately predict many properties such as solubility, activity coefficient, and diffusivity [71-72], while the integration of TIP4P/2005 and Madrid-2019 leads to more accurate prediction of solubility, density, viscosity and other structural properties [71-73]. The augmented OPLS-AA force field [65] is used for toluene and C5Pe, with bond length and bond angle each described by a harmonic potential, and dihedral angle describe by the Ryckaert-Bellemans function [65]. The force field parameters are generated from the LigParGen web server [74]. The partial charges for these molecules are re-parameterized using the 1.14×CM1A-LBCC algorithm [75], which improves the accuracy of prediction for the heat of vaporization and density of organic liquids [75]. Prior simulations have validated the accuracy of the force field parameters in modeling toluene, against experimental data [ref]. By performing an auxiliary *NPT* simulation that equilibrates 1000 C5Pe molecules at 300 K and 1 bar, the density of C5Pe in this work is calculated to be 1116.77 ± 3.03 kg/m^3, which agrees well with previous simulation result (1121.54 ± 2.68 kg/m^3 calculated by GROMOS force field) [6].

Water molecules are kept rigid by the SETTLE algorithm [76] and bond lengths involving an H atom are fixed in toluene and C5Pe via the LINCS algorithm [77]. The velocity rescaling thermostat [78] with a time constant of 0.5 ps is used to control the temperature. Three-dimensional PBCs are applied. Lennard-Jones potential is truncated at 1.2 nm with tail correction [79]. The long-range electrostatic interaction is handled by the particle-mesh Ewald (PME) method [80]. To further screen the long-range interaction between the system and its images in *z*-direction, a force and potential correction is applied in the *z*-direction to produce a pseudo two-dimensional Ewald summation (ewald-geometry set as “3dc” in the mdp file). The time step is 1 fs throughout all the simulations, and the trajectory is saved every 2 ps for the sampling stage.

3. Results and Discussion

3.1. Salt Ions Stabilize Droplet

Figures 2(a)-(d) presents the equilibrium radial density (ρ) profiles of all the fluid components in System S0 under different electric fields. The horizontal axis (r) is the distance from the COM of the water droplet. The band with a lighter color surrounding each curve represents the standard deviation from the statistical analysis of data. Regardless of the electric field strength, the density of C5Pe molecules shows a clear peak near the water-toluene interface corresponding to their adsorption. This is expected because C5Pe is amphiphilic, which tends to interact with both water and oil phases [6, 81-82]. On the other hand, as the electric field strength increases, the plateau region in the water density profile at small r becomes narrower, which suggests size or geometry changes of the water droplet. **Figures 2(e)-(h)** are the time-averaged three-dimensional iso-density surfaces for water and C5Pe, providing a more direct view of the droplet deformation and C5Pe distribution. In each plot, the atomic coordinates are shifted so that the COM of the water droplet is at the center of the x-y plane (no shifting in the z direction). The iso-values for water and C5Pe are respectively set to 500 kg/m^3 and 280 kg/m^3. As depicted, the water droplet is spherical at $E = 0$ V/nm, but gradually elongates along the z-direction (the direction of electric field) to an ellipsoid at $E = 0.5$ V/nm, a spindle at $E = 0.75$ V/nm, and finally a cylinder at $E = 1.0$ V/nm. The stretching of water droplet along the electric field has been reported in previous studies [38-51], and is caused by the balance between surface and electrostatic forces as elaborated in the literature [6, 23, 29-30]. It should be pointed out that the distance between the two electrodes is 20 nm in the simulations, which is much smaller that in experiments. With larger distances the cylindrical-shaped droplet shown in **Figures 2(h)** is likely unstable and tends to break up, as observed in experiments [19, 23, 29, 36-37]. However, such an artifact, caused by the limited length scale in MD simulations, is only present when the droplet is simultaneously interacting with both electrodes, which is rarely observed in the simulations.

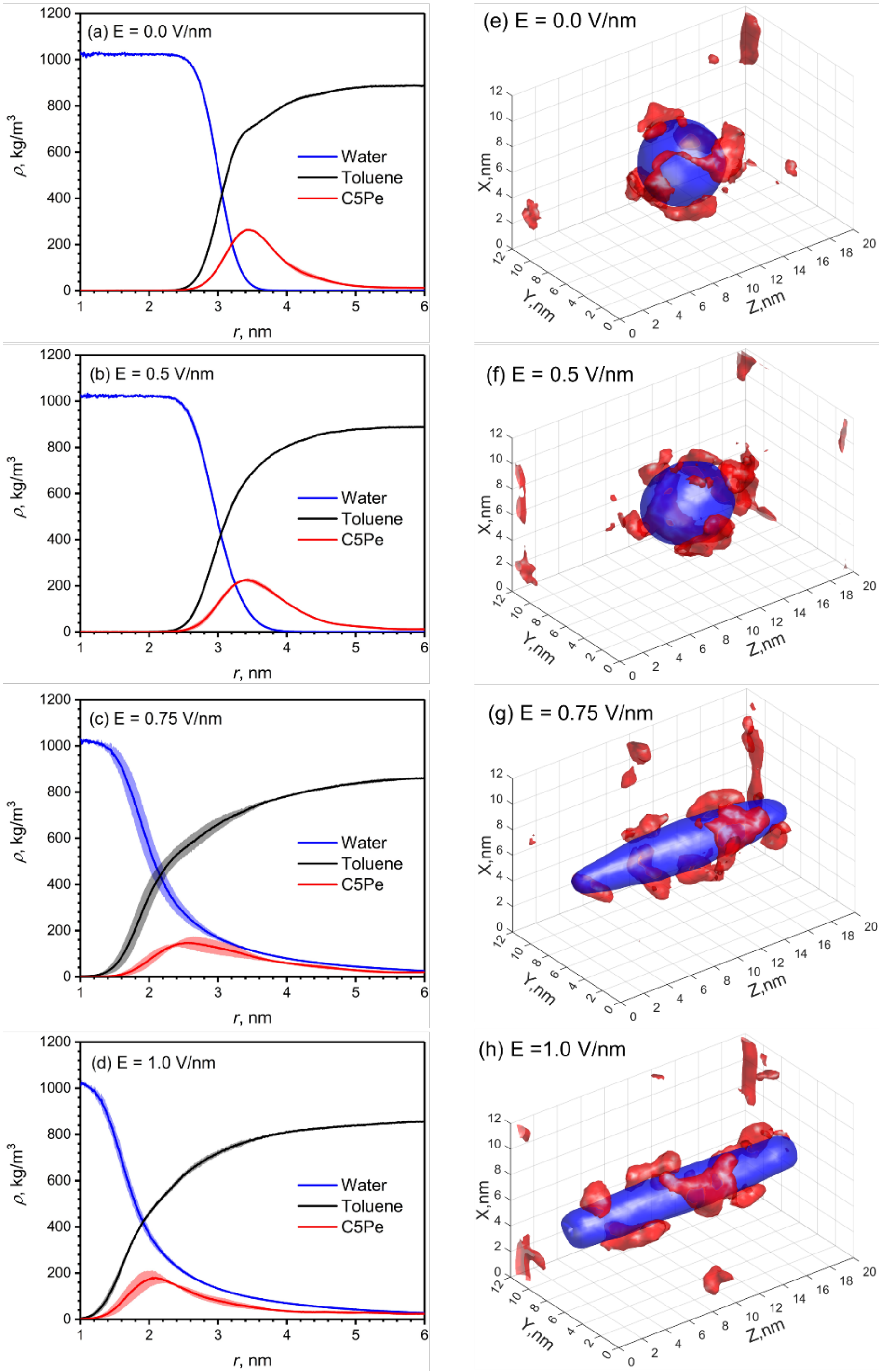

Figure 2 (a)-(d): Equilibrium radial density profiles of fluid components in System S0 under different electric field strengths, with *r* being the distance from COM of the water droplet. (e)-(h): Corresponding three-dimensional iso-density surfaces for water (blue, iso-density = 500 kg/m^3) and C5Pe (red, iso-density = 280 kg/m^3).

The presence of salt ions in the water droplet has a significant effect on its stability under electric field. To demonstrate this, the equilibrium radial density of the fluid components and their iso-density surfaces are depicted in **Figures 3** for System S4_Ca containing 4.5 wt% of $CaCl_2$. In contrast to **Figure 2**, the changes in the density profiles induced by the electric field are much smaller, suggesting that the droplet is able to maintain a spherical or ellipsoid shape even for $E \geq 0.75$ V/nm. In **Figure 3**, the iso-density surfaces of salt ions (0.25 mol/L for Ca^{2+} and 0.5 mol/L for Cl^{-}) are also shown. At high electric field strengths ($E \geq 0.75$ V/nm), some Ca^{2+} and Cl^{-} ions hydrated by small water clusters are found to leave the water droplet and move towards the anode and cathode, respectively. In **Figures 3(g)** and **3(h)**, considerable number of salt ions are attached to the electrodes inducing an electric field that is opposite to the originally applied electric field. This screening effectively reduces the electric field experienced by the water droplet, allowing it to maintain a spherical or ellipsoid shape. To further quantify the screening effect brought by the salt ions, **Figure 4(a)** shows for System S4_Ca the electric field induced by salt ions (E_{ind}) after system equilibration, where E_{ind} is calculated by integrating the charge distribution of salt ions. **Figure 4(b)** shows the net electric field (E_{net}) after summing the applied E and E_{ind}. For $E = 0.75$ V/nm and 1.0 V/nm, E_{net} drops to ~ 0.4 V/nm approximately 1−2 nm from the electrodes, which is not strong enough to cause a significant deformation of the brine droplet. E_{ind} and E_{net} for other systems are shown in **Figure S1-S7** in the Supporting Information (SI), which are similar to **Figure 4**. Therefore, the roles of salt ions are two-fold. On the one hand, as they move towards the electrodes, they bring the hydrating water molecules with them, which facilitate droplet breakup. On the other hand, they reduce the effective electric field which stabilizes the main body of the emulsion droplet, preventing it from large deformations. Li et al. also reported the former effect in their series of works [49-51] but not the second role. In fact, the electrodes were absent in Li et al. [49-51] due to different system setup.

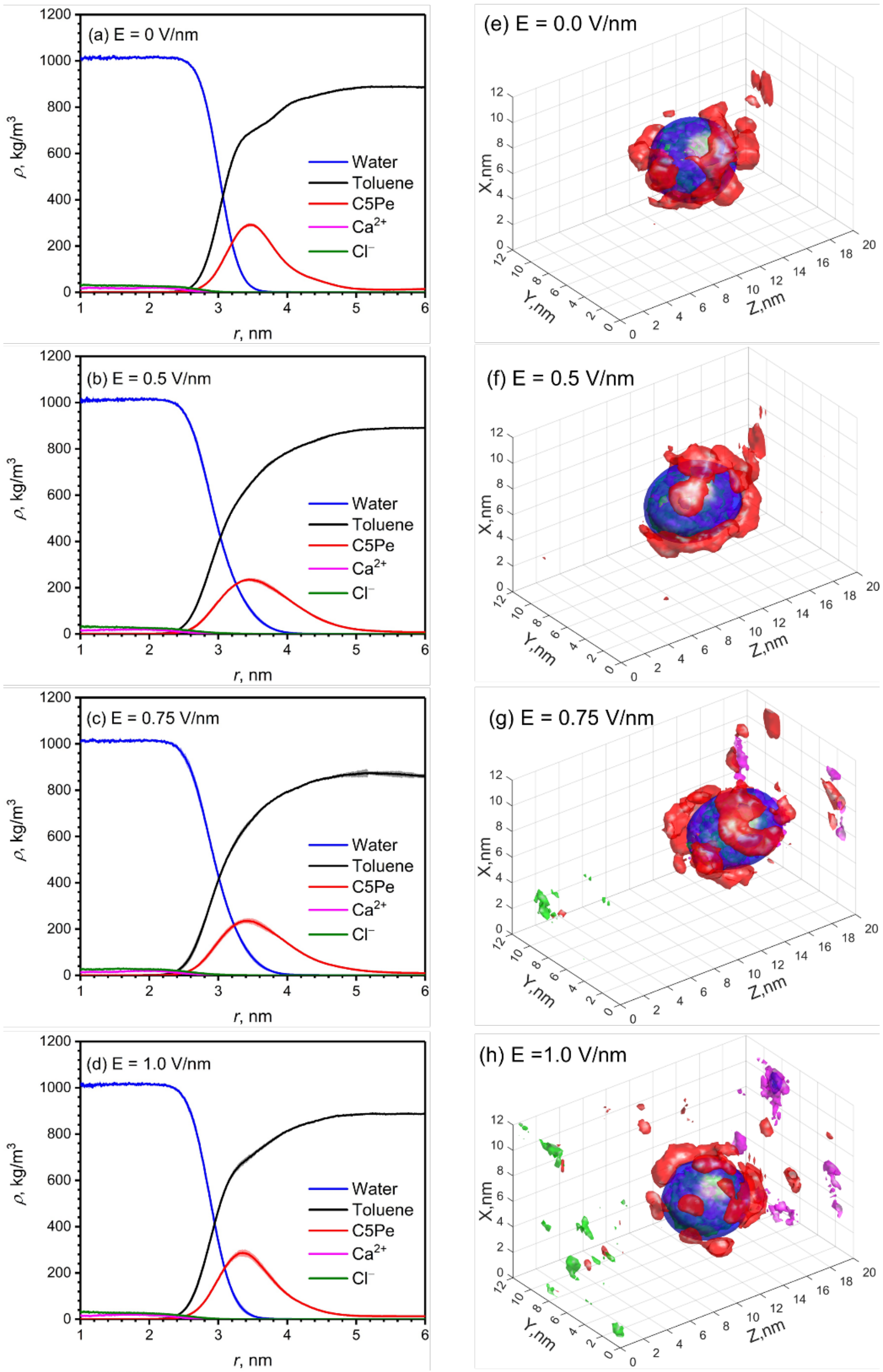

Figure 3 (a)-(d): Equilibrium radial density profiles of fluid components in System S4_Ca under different electric field strengths. (e)-(h): Corresponding three-dimensional iso-density surfaces for

water (blue, iso-density = 500 kg/m^3), C5Pe (red, iso-density = 280 kg/m^3), Ca^{2+} (magenta, iso-density = 10 kg/m^3, i.e., 0.25 mol/L), and Cl$^-$ (green, iso-density = 17.725 kg/m^3, i.e., 0.5 mol/L).

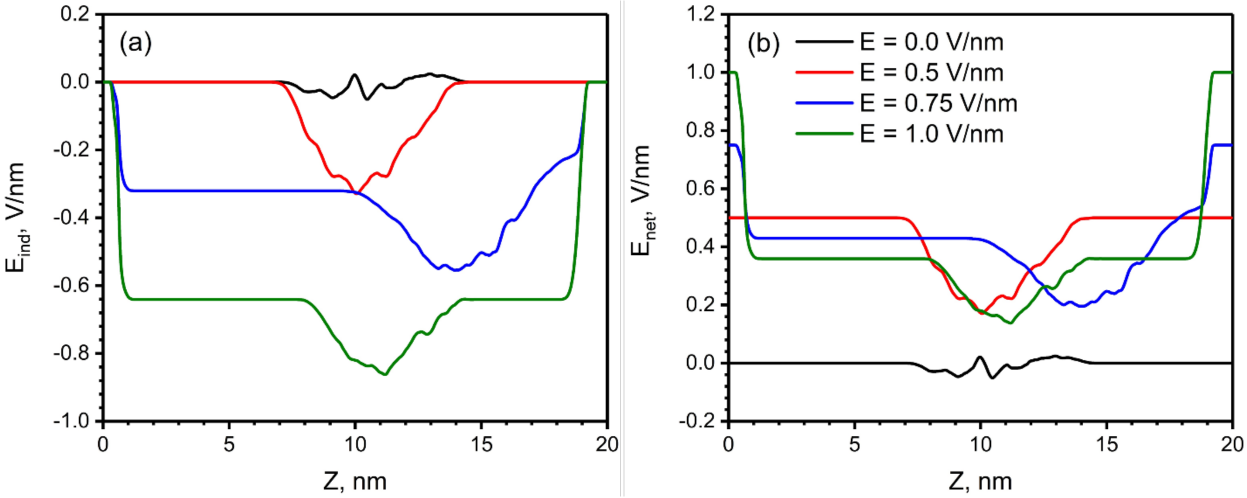

Figure 4 (a) Electric field induced by salt ions, E_{ind}; and (b) the net electric field, $E_{net} = E + E_{ind}$ in System S4_Ca after equilibration.

3.2. NaCl and CaCl$_2$ Droplets Behave Differently at Low Concentration

Figure 5 shows the equilibrium radial density profiles and three-dimensional iso-density surfaces for System S4_Na. It is the counterpart of **Figure 3** (for System S4_Ca), but with Ca^{2+} replaced by Na$^+$. The corresponding plots for the other systems in **Table 1** are shown in **Figures S8-S13**. In **Figure 5**, at high electric field strengths ($E \geq 0.75$ V/nm), some of the salt ions become attached to the electrodes, similar to the observation in System S4_Ca. On the other hand, it is interesting to find that when $E \geq 0.75$ V/nm, the main body of NaCl droplet adheres to one electrode, while the main body of CaCl$_2$ droplet remains in the bulk oil. **Figure 6** compares the evolution of the droplet in the two systems during the equilibration stage. In System S4_Ca, while under the electric field of $E = 1.0$ V/nm a fraction of ions and their surrounding water molecules are ejected from the two ends of the droplet, the COM of the CaCl$_2$ droplet remains almost unchanged in the z-direction. On the contrary, in System S4_Na, after ejecting some Na^+ ions from the right end, the COM of the NaCl droplet gradually moves to the left, and finally a large fraction of the droplet adheres to the left electrode. The evolutions of droplet deformation in other systems are shown in **Figures S14-S16**. It is found that the above phenomenon only occurs when the NaCl concentration is less than 7.8 wt%, whereas the deformation of NaCl droplet resembles that of $CaCl_2$ droplet (COM remains unchanged) when the NaCl concentration is higher. This effect of salt concentration is discussed next.

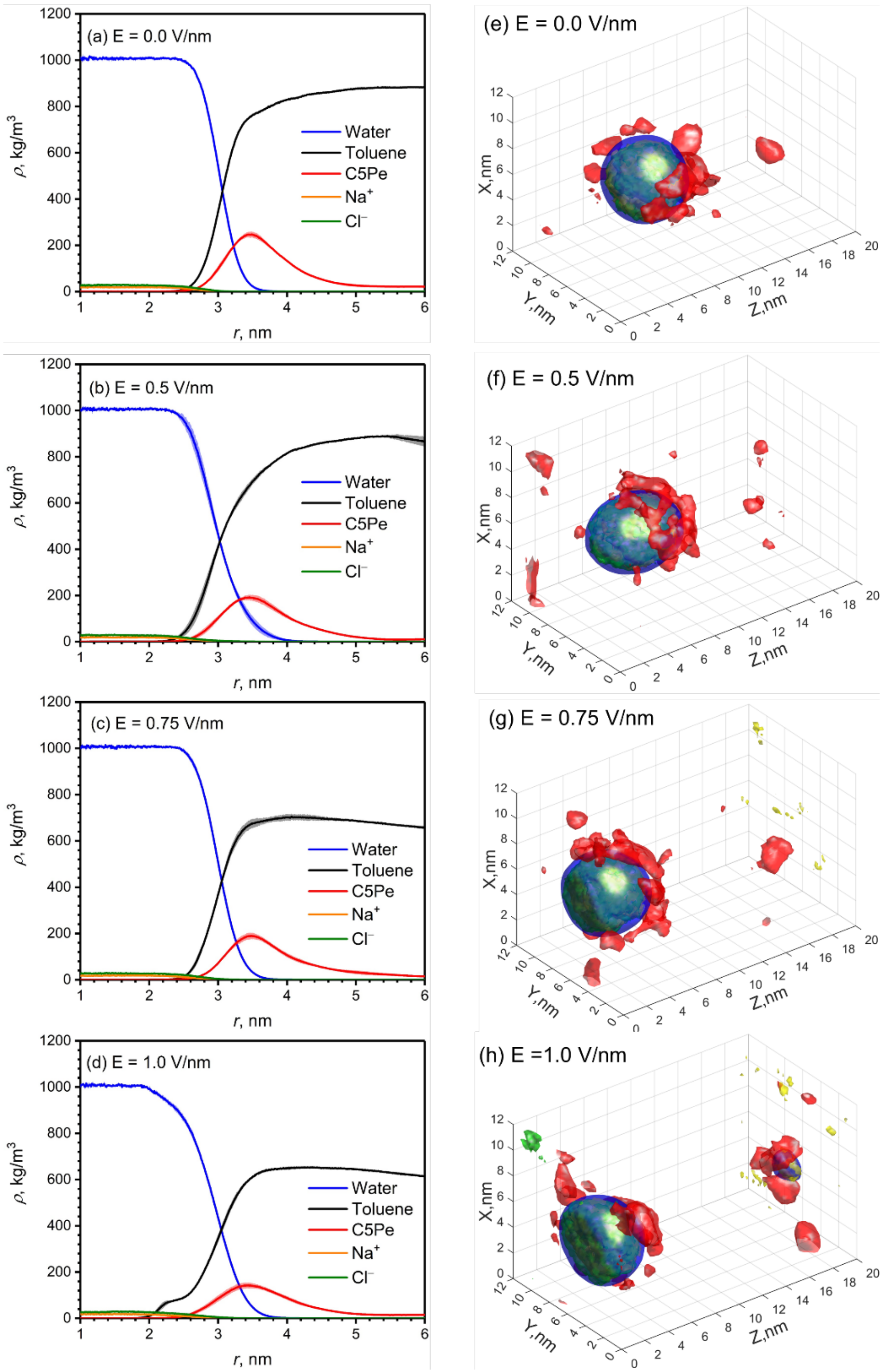

Figure 5 (a)-(d): Equilibrium radial density profiles of fluid components in System S4_Na under different electric field strengths. (e)-(h): Corresponding three-dimensional iso-density surface for water (blue, iso-density = 500 kg/m^3), C5Pe (red, iso-density = 280 kg/m^3), Na$^+$ (yellow, iso-density = 11.5 kg/m^3, i.e., 0.5 mol/L), and Cl$^-$ (green, iso-density = 17.725 kg/m^3, i.e., 0.5 mol/L).

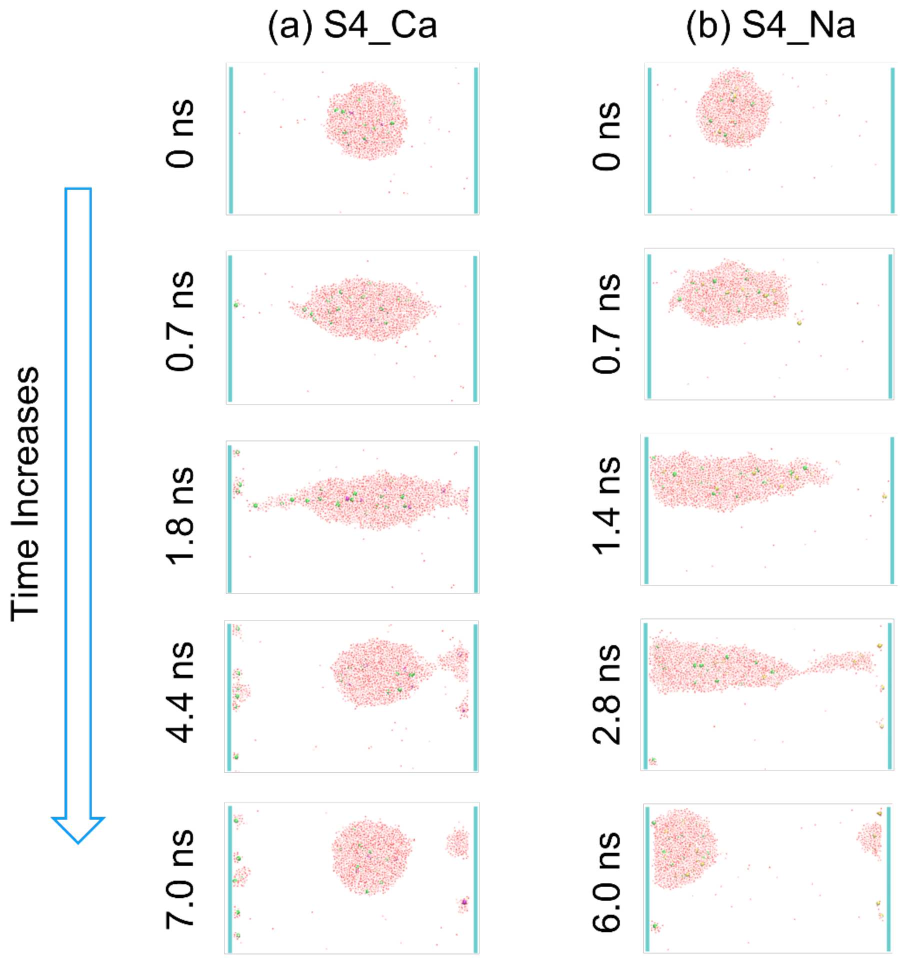

Figure 6 Time evolution of droplet deformation under *E* = 1.0 V/nm: (left panel) System S4_Ca and (right panel) System S4_Na. *t* = 0 ns corresponds to when the electric field is just applied. The location and shape of the droplets are stabilized with little change after the last frame shown in the figure.

3.3. Salt Concentration Affects Droplet Stability under High Electric Field

Combining **Figures 6** and **S14-S16**, it is fount that when the NaCl concentration is higher than a certain value (between 4.5 wt% and 7.8 wt%), a large fraction of the brine droplet remains in bulk oil even under a high electric field ($E \geq 0.75$ V/nm). Interestingly, when the electric field is applied, the droplet deforms into a spindle, ejects Na^+ and Cl^- ions from the two ends, and then recovers it spherical shape as the screening of the electric field by the salt ions takes place (see **Figures S15-S16**). However, if the NaCl concentration is below this value, under the same electric field, the droplet undergoes significant deformation while simultaneously drifting towards an electrode. When the salt is $CaCl_2$, within the studied range of concentrations (from 2.5 wt% to 11.4 wt%), the brine droplet always stays in bulk oil, similar to the scenario with high concentrations of NaCl.

To explore the mechanism behind this phenomenon, **Figure 7** shows time evolution of the net charge carried by the brine droplet during equilibration, under E = 0.75 and 1.0 V/nm. The net charge exhibits large fluctuations when the electric field is just applied (within the first 5 ns). During this period, the droplet undergoes drastic deformation, and the ions are ejected from the ends of the droplet. After this period, the net charge becomes stable with minor fluctuations. It is suspected that the NaCl droplets at low salt concentrations move towards an electrode due to their non-zero net charge, which leads to an electrical force on the droplet. The data in **Figure 7** are partially consistent with this hypothesis. For example, in System S4_Na, the stabilized net charge is -2.55 e for E = 0.75 V/nm and -5.95 e for E = 1.0 V/nm, and these two droplets finally drift to the cathode under the electric field. In addition, the NaCl droplet in System S2_Na under E = 1.0 V/nm carries a positive charge (+5.95 e) in the stable period, and it diffuses to the anode. In contrast, when the NaCl concentration increases to ≥ 7.8 wt %, the net charge of the droplet converges to around zero and its tendency towards an electrode is not observed. It should be noted, however, several data in **Figure 7** cannot be fully explained by the droplet's net charge. Specifically, the droplet in System S2_Na under E = 0.75 V/nm has a similar net charge to the droplets in Systems S2_Ca and S11_Ca under E = 0.75 and 1.0 V/nm, System S4_Ca under E = 0.75 V/nm, System

S7_Ca under $E = 1.0$ V/nm, as well as System S11_Na under $E = 1.0$ V/nm, but it is the only one that adheres to an electrode after equilibration.

The seeming discrepancy can be explained by the strength of C5Pe adsorption on the brine droplet. For this purpose, umbrella sampling (US) is employed to determine the potential of mean force (PMF) of a single C5Pe molecule as a function of the distance (ζ) between its COM and a brine-toluene interface, under salt concentrations that are close to those listed in **Table 1.** An example of the system setup is shown in **Figure 8(a).** $\zeta = 0$ is defined by the position where the water density is 50% of its bulk value in the brine phase. Each US simulation is run for 30 ns and data from the last 20 ns are analyzed using the weighted histogram analysis method (WHAM) [83] to obtain the PMF profile. Other details of the PMF calculations can be found in **SI Section S4**. **Figure 8(b)** summarizes the PMF curves for the NaCl brine-toluene systems, where the depth of the PMF well is a quantitative measure of the strength of C5Pe adsorption. The adsorption strength shows a generally increasing trend with the NaCl concentration: 0 wt % < 2.1 wt % ≈ 4.8 wt % < 8.5 wt % ≈ 11.7 wt %. The corresponding results are shown in **Figure 8(c)** for $CaCl_2$ brine-toluene systems. Interestingly, the strongest interaction between C5Pe and $CaCl_2$ brine occurs at 2.3 wt%. From 2.3 wt% to 8.4 wt% the adsorption strength decreases, but it increases again as the salt concentration further increases to 11.6 wt%. Stronger C5Pe-brine interaction could induce a higher amount of C5Pe adsorption on the brine droplet surface, which is confirmed in **Figure 8(d)** for the systems simulated in **Table 1** at $E = 0$ V/nm. The number of adsorbed C5Pe is calculated by performing a volume integration of the radial density (**Figures 2**, **3**, **5**, and **S8-S13**) from $r = 0$ to $r = 5$ nm. The number of adsorbed C5Pe on the NaCl droplet shows an overall increasing trend with NaCl concentration. In contrast, the highest adsorption on the $CaCl_2$ droplet occurs at 2.3 wt%, followed by a drop from 2.3 wt% to 4.8 wt% and a slight increase afterwards. Both curves agree well with the PMF results. Higher amount of C5Pe adsorption leads to greater mass (hence inertia) and larger volume (hence viscous drag) of the droplet as a whole, making it more difficult to move in the bulk oil. Consequently, although several brine droplets (Systems S2_Ca and S11_Ca under $E = 0.75$ and 1.0 V/nm, System S4_Ca under $E = 0.75$ V/nm, System S7_Ca under $E = 1.0$ V/nm, System S11_Na under $E = 1.0$ V/nm) have a net charge comparable to the NaCl droplet in System S2_Na under $E = 0.75$ V/nm, the latter has relatively low C5Pe adsorption, which enables its easier movement towards an electrode. Therefore, the motion of the droplet under an electric field is a result of the collective effects of the droplet net charge and C5Pe adsorption.

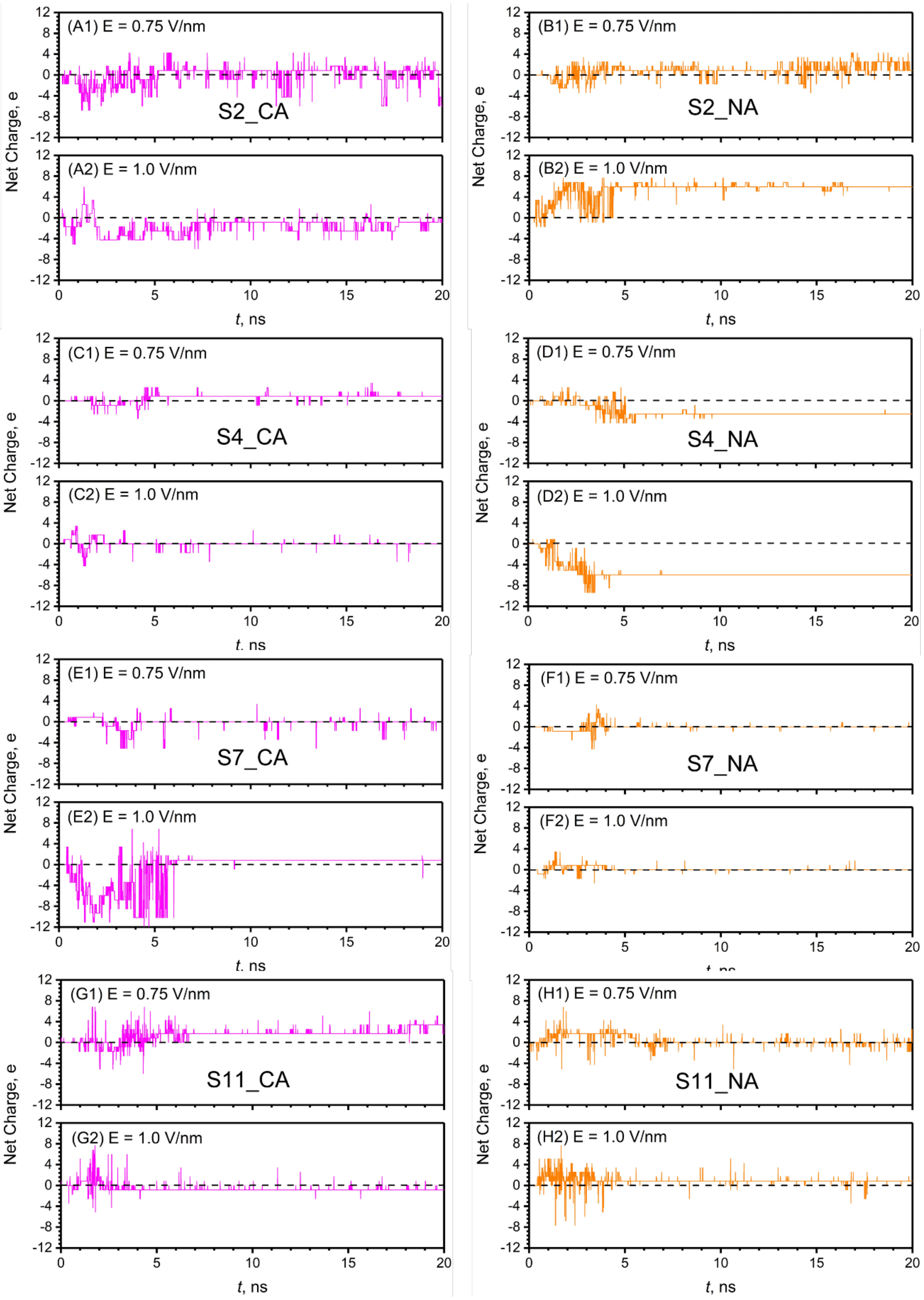

Figure 7 Time evolution of the net charge of the brine droplet during the equilibration stage.

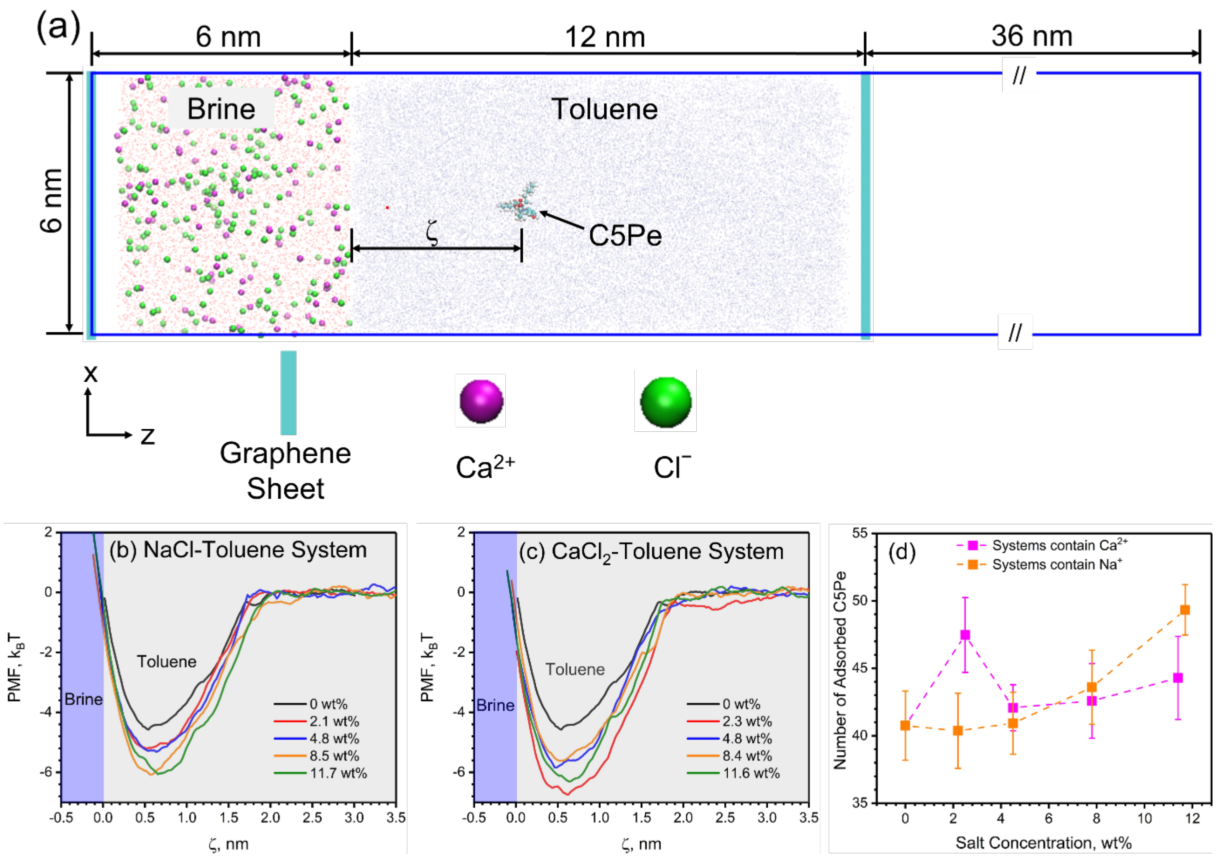

Figure 8 (a) An example ($CaCl_2$-toluene system with salt concentration of 8.4 wt%) of the initial configuration for PMF calculation. PMF profiles along the reaction coordinate ζ (distance between COM of C5Pe and brine-toluene interface) in (b) NaCl brine-toluene systems and (c) $CaCl_2$ brine-toluene systems with different salt concentrations. (d) Number of C5Pe molecules adsorbed on the brine droplet surface at $E = 0$ V/nm, plotted against salt concentration.

3.4. Implications in Electrostatic Demulsification

Figure 9 summarizes the stability of the brine droplet found in this work into phase diagrams with salt concentration and cation valency as the two axes. A droplet is considered stable if it remains approximately a spherical shape and stays in bulk oil. In contrast, an unstable droplet either deforms into a cylinder or becomes attached to an electrode. When the electric field is small (0 to 0.5 V/nm), the droplet simulated here is stable regardless of the salt concentration and cation valency (**Figure 9(a)**). At higher electric field (0.75 to 1.0 V/nm in this work), the droplet is unstable in two systems with monovalent ions and small salt concentrations. Therefore, a boundary can be drawn to separate an unstable regime from a stable one (**Figure 9(b)**). It is expected that as the electric field increases, this boundary would move in the upper-right direction, increasing the size of the unstable regime. **Figure 9** is generated from the simulation results on NaCl and $CaCl_2$ brine droplets. Although a major distinction between the two types of salt is the valency of the cations, there are other differences such as the mass and hydration free energy of the cations, as well as the binding free energy between the cation and anion. The same phase diagrams may not be applicable to other salt ions (e.g., K^+ or Mg^{2+}) and should be evaluated with additional simulations.

The comparison in Section 3.1 suggests that the presence of salt ions in water-in-oil emulsion could lower the efficacy of demulsification by electric field. The ions induce a counter electric field that weakens the originally applied field, as well the detachment of salt ions and their surrounding water molecules from the emulsion droplets generates tiny daughter droplets which also creates a barrier for demulsification. In addition, as seen in Section 3.3, salt ions could strengthen the interaction between brine droplets and asphaltenes in the crude oil, which is unfavorable for demulsification. Therefore, removing the salt ions could be a complementary means to help increase the efficacy of electric field based demulsification.

Section 3.2 shows that the droplet containing Ca^{2+} ions are more stable than that with Na^+ ions. Interestingly, a non-monotonic relationship is found in Section 3.3 between C5Pe adsorption and $CaCl_2$ concentration. Similar phenomena related to Ca^{2+} were also reported in previous literature [53-56]. For example, Morrow and Buckley reported that the oil recovery could be enhanced by injecting brine with low salinity, but this effect disappeared when the salinity of injected water is too high or too low [53]. The benefit of this so-called "low salinity water flooding" was attributed to the complex interaction among Ca^{2+}, polar components in crude oil, and rock surface [54-56]. Therefore, special care should be exercised when treating water-in-oil emulsion systems containing Ca^{2+}.

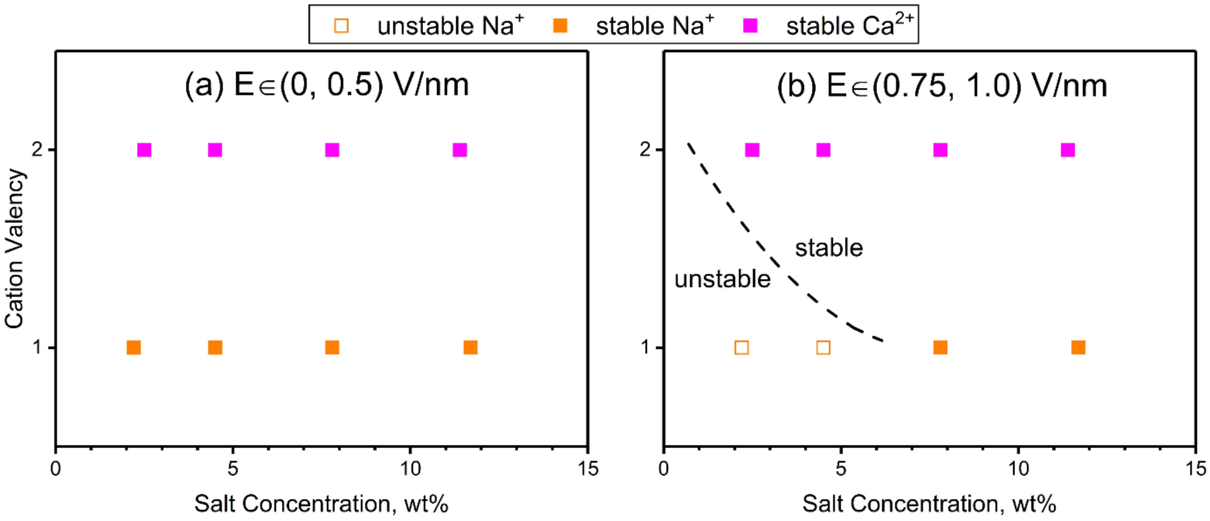

Figure 9 Schematic phase diagrams of brine droplet stability in oil under (a) $E \in (0, 0.5)$ V/nm and (b) $E \in (0.75, 1.0)$ V/nm, with salt concentration and cation valency serving as the axes of the phase diagrams.

4. Conclusion

MD simulations are conducted to investigate the stability of a NaCl or $CaCl_2$ brine droplet in a model oil when exposed to an external electric field. It is found that the presence of salt ions helps the brine droplet maintain a spherical shape under high electric field strengths (≥ 0.75 V/nm), while the bare water droplet deforms into a spindle or cylinder under the same electric field. The contrasting behaviors are caused by some salt ions departing from the droplet towards the electrodes, which generates a counter electric field and reduces the effective strength of the external electric field. The brine droplet also exhibits different deformation and motion in the systems containing Na^+ and Ca^{2+}. With Na^+, if the salt concentration is less than a threshold (between 4.4 wt% and 7.7 wt%) the main body of the droplet tends to attach to an electrode, while it remains in the bulk oil if the salt concentration is higher than the threshold. With Ca^{2+}, within the studied salt concentration range, the brine droplet always stays in the bulk oil. We attribute this difference to both the net charge of the droplet and C5Pe adsorption on the droplet surface. High net charge and low C5Pe adsorption at low salt concentration lead the NaCl droplet towards an electrode, while increased C5Pe adsorption with NaCl concentration reduces the drift. $CaCl_2$ droplet has a low net charge and relatively high C5Pe adsorption, which limits its tendency to leave the bulk oil. From practical point of view, removing salt ions could facilitate demulsification by electric field, and special attention should be paid to salt ions (e.g., Ca^{2+}) that provide higher stability to the emulsion droplets.

Associated Content

Supporting Information. Counter Electric Field by Ions, Radial Density and Three-dimensional Iso-density Surface Plots, Evolution of Droplet Deformation, and Potential of Mean Force (PMF) Calculations.

Conflict of Interest

The authors declare no conflict of interest.

Acknowledgements

The authors gratefully acknowledge the computing resources and technical support from the Digital Research Alliance of Canada, and the financial support from the Natural Sciences and Engineering Research Council of Canada (NSERC), Syncrude Canada Ltd., Suncor Energy, Canadian Natural Resources Limited, ChampionX, the Canada Research Chairs Program, and the Future Energy Systems under the Canada First Research Excellence Fund.

References

(1) Wang, D.; Yang, D.; Huang, C.; Huang, Y.; Yang, D.; Zhang, H.; Liu, Q.; Tang, T.; El-Din, M. G.; Kemppi, T. Stabilization Mechanism and Chemical Demulsification of Water-in-Oil and Oil-in-Water Emulsions in Petroleum Industry: A Review. *Fuel* **2021**, *286*, 119390.

(2) Sun, X.; Yang, D.; Zhang, H.; Zeng, H.; Tang, T. Unraveling the Interaction of Water-in-Oil Emulsion Droplets Via Molecular Simulations and Surface Force Measurements. *J. Phys. Chem. B* **2021**, *125* (27), 7556-7567.

(3) Sun, X.; Zeng, H.; Tang, T. Effect of Non-Ionic Surfactants on the Adsorption of Polycyclic Aromatic Compounds at Water/Oil Interface: A Molecular Simulation Study. *J. Colloid Interface Sci.* **2021**, *586*, 766-777.

(4) Lu, H.; Pan, Z.; Miao, Z.; Xu, X.; Wu, S.; Liu, Y.; Wang, H.; Yang, Q. Combination of Electric Field and Medium Coalescence for Enhanced Demulsification of Oil-in-Water Emulsion. *Chemical Engineering Journal Advances* **2021**, *6*, 100103.

(5) Xu, Y.; Dabros, T.; Hamza, H. Study on the Mechanism of Foaming from Bitumen Froth Treatment Tailings. *J. Dispersion Sci. Technol.* **2007**, *28* (3), 413-418.

(6) Li, W.; Zeng, H.; Tang, T. Molecular Dynamics Simulation on Water/Oil Interface with Model Asphaltene Subjected to Electric Field. *J. Colloid Interface Sci.* **2022**, *628*, 924-934.

(7) Issaka, S. A.; Nour, A. H.; Yunus, R. M. Review on the Fundamental Aspects of Petroleum Oil Emulsions and Techniques of Demulsification. *Journal of Petroleum & Environmental Biotechnology* **2015**, *6* (2), 1.

(8) Umar, A. A.; Saaid, I. B. M.; Sulaimon, A. A.; Pilus, R. B. M. A Review of Petroleum Emulsions and Recent Progress on Water-in-Crude Oil Emulsions Stabilized by Natural Surfactants and Solids. *Journal of Petroleum Science and Engineering* **2018**, *165*, 673-690.

(9) Raya, S. A.; Saaid, I. M.; Ahmed, A. A.; Umar, A. A. A Critical Review of Development and Demulsification Mechanisms of Crude Oil Emulsion in the Petroleum Industry. *Journal of Petroleum Exploration and Production Technology* **2020**, *10* (4), 1711-1728.

(10) Mhatre, S.; Simon, S.; Sjöblom, J. Shape Evolution of a Water Drop in Asphaltene Solution under Weak Dc Electric Fields. *Chem. Eng. Res. Des.* **2019**, *141*, 540-549.

(11) Mhatre, S.; Simon, S.; Sjöblom, J. Experimental Evidence of Enhanced Adsorption Dynamics at Liquid–Liquid Interfaces under an Electric Field. *Anal. Chem.* **2020**, *92* (19), 12860-12870.

(12) Li, W.; Nan, Y.; Wen, X.; Wang, W.; Jin, Z. Effects of Salinity and N-, S-, and O-Bearing Polar Components on Light Oil–Brine Interfacial Properties from Molecular Perspectives. *J. Phys. Chem. C* **2019**, *123* (38), 23520-23528.

(13) Li, W.; Nan, Y.; You, Q.; Jin, Z. Co2 Solubility in Brine in Silica Nanopores in Relation to Geological Co2 Sequestration in Tight Formations: Effect of Salinity and Ph. *Chem. Eng. J.* **2021**, *411*, 127626.

(14) Ichikawa, T. Electrical Demulsification of Oil-in-Water Emulsion. *Colloids and Surfaces A: Physicochemical and Engineering Aspects* **2007**, *302* (1-3), 581-586.

(15) Mohammadian, E.; Taju Ariffin, T. S.; Azdarpour, A.; Hamidi, H.; Yusof, S.; Sabet, M.; Yahya, E. Demulsification of Light Malaysian Crude Oil Emulsions Using an Electric Field Method. *Industrial & Engineering Chemistry Research* **2018**, *57* (39), 13247-13256.

(16) Ren, B.; Kang, Y. Demulsification of Oil-in-Water (O/W) Emulsion in Bidirectional Pulsed Electric Field. *Langmuir* **2018**, *34* (30), 8923-8931.

(17) Mhatre, S.; Hjartnes, T.; Simon, S.; Sjöblom, J. Coalescence Behavior of Stable Pendent Drop Pairs Held at Different Electric Potentials. *Langmuir* **2020**, *36* (7), 1642-1650.

(18) Sjöblom, J.; Mhatre, S.; Simon, S.; Skartlien, R.; Sørland, G. Emulsions in External Electric Fields. *Adv. Colloid Interface Sci.* **2021**, *294*, 102455.

(19) Torza, S.; Cox, R.; Mason, S. Electrohydrodynamic Deformation and Bursts of Liquid Drops. *Philosophical Transactions of the Royal Society of London. Series A, Mathematical and Physical Sciences* **1971**, *269* (1198), 295-319.

(20) Taylor, G. I. Studies in Electrohydrodynamics. I. The Circulation Produced in a Drop by an Electric Field. *Proceedings of the Royal Society of London. Series A. Mathematical and Physical Sciences* **1966**, *291* (1425), 159-166.

(21) Zeleny, J. Instability of Electrified Liquid Surfaces. *Phys. Rev.* **1917**, *10* (1), 1.

(22) Allan, R.; Mason, S. Particle Behaviour in Shear and Electric Fields I. Deformation and Burst of Fluid Drops. *Proceedings of the Royal Society of London. Series A. Mathematical and Physical Sciences* **1962**, *267* (1328), 45-61.

(23) Taylor, G. I. Disintegration of Water Drops in an Electric Field. *Proceedings of the Royal Society of London. Series A. Mathematical and Physical Sciences* **1964**, *280* (1382), 383-397.

(24) Moran, K.; Yeung, A.; Masliyah, J. Measuring Interfacial Tensions of Micrometer-Sized Droplets: A Novel Micromechanical Technique. *Langmuir* **1999**, *15* (24), 8497-8504.

(25) Yeung, A.; Dabros, T.; Masliyah, J. Does Equilibrium Interfacial Tension Depend on Method of Measurement? *J. Colloid Interface Sci.* **1998**, *208* (1), 241-247.

(26) Goebel, A.; Lunkenheimer, K. Interfacial Tension of the Water/N-Alkane Interface. *Langmuir* **1997**, *13* (2), 369-372.

(27) Yang, Y.; Nair, A. K. N.; Ruslan, M. F. A. C.; Sun, S. Interfacial Properties of the Aromatic Hydrocarbon+ Water System in the Presence of Hydrophilic Silica. *J. Mol. Liq.* **2022**, *346*, 118272.

(28) Li, W.; Jin, Z. Molecular Dynamics Simulations of Natural Gas-Water Interfacial Tensions over Wide Range of Pressures. *Fuel* **2019**, *236*, 480-492.

(29) Abbasi, M. S.; Song, R.; Kim, S.-M.; Kim, H.; Lee, J. Mono-Emulsion Droplet Stretching under Direct Current Electric Field. *Soft Matter* **2019**, *15* (11), 2328-2335.

(30) Luo, X.; Yan, H.; Huang, X.; Yang, D.; Wang, J.; He, L. Breakup Characteristics of Aqueous Droplet with Surfactant in Oil under Direct Current Electric Field. *J. Colloid Interface Sci.* **2017**, *505*, 460-466.

(31) Garton, C.; Krasucki, Z. Bubbles in Insulating Liquids: Stability in an Electric Field. *Proceedings of the Royal Society of London. Series A. Mathematical and Physical Sciences* **1964**, *280* (1381), 211-226.

(32) Ajayi, O. A Note on Taylor's Electrohydrodynamic Theory. *Proceedings of the Royal Society of London. A. Mathematical and Physical Sciences* **1978**, *364* (1719), 499-507.

(33) Gong, H.; Peng, Y.; Shang, H.; Yang, Z.; Zhang, X. Non-Linear Vibration of a Water Drop Subjected to High-Voltage Pulsed Electric Field in Oil: Estimation of Stretching Deformation and Resonance Frequency. *Chem. Eng. Sci.* **2015**, *128*, 21-27.

(34) Berg, G.; Lundgaard, L. E.; Abi-Chebel, N. Electrically Stressed Water Drops in Oil. *Chemical Engineering and Processing: Process Intensification* **2010**, *49* (12), 1229-1240.

(35) Ervik, Å.; Penne, T. E.; Hellesø, S. M.; Munkejord, S. T.; Müller, B. Influence of Surfactants on the Electrohydrodynamic Stretching of Water Drops in Oil. *Int. J. Multiphase Flow* **2018**, *98*, 96-109.

(36) Karyappa, R. B.; Thaokar, R. M. Electric-Field-Assisted Formation of Nonspherical Microcapsules. *Langmuir* **2014**, *30* (34), 10270-10279.

(37) Dubash, N.; Mestel, A. J. Breakup Behavior of a Conducting Drop Suspended in a Viscous Fluid Subject to an Electric Field. *Phys. Fluids* **2007**, *19* (7), 072101.

(38) Wang, Z.; Li, N.; Sun, Z.; Wang, X.; Chen, Q.; Liu, W.; Qi, Z.; Wei, L.; Li, B. Molecular Dynamics Study of Droplet Electrocoalescence in the Oil Phase and the Gas Phase. *Sep. Purif. Technol.* **2021**, *278*, 119622.

(39) Wang, B.-B.; Wang, X.-D.; Yan, W.-M.; Wang, T.-H. Molecular Dynamics Simulations on Coalescence and Non-Coalescence of Conducting Droplets. *Langmuir* **2015**, *31* (27), 7457-7462.

(40) Song, F.; Niu, H.; Fan, J.; Chen, Q.; Wang, G.; Liu, L. Molecular Dynamics Study on the Coalescence and Break-up Behaviors of Ionic Droplets under Dc Electric Field. *J. Mol. Liq.* **2020**, *312*, 113195.

(41) He, X.; Wang, S.-L.; Yang, Y.-R.; Wang, X.-D.; Chen, J.-Q. Electro-Coalescence of Two Charged Droplets under Pulsed Direct Current Electric Fields with Various Waveforms: A Molecular Dynamics Study. *J. Mol. Liq.* **2020**, *312*, 113429.

(42) Wang, B.-B.; Wang, X.-D.; Wang, T.-H.; Lu, G.; Yan, W.-M. Electro-Coalescence of Two Charged Droplets under Constant and Pulsed Dc Electric Fields. *Int. J. Heat Mass Transfer* **2016**, *98*, 10-16.

(43) Wang, B.-B.; Wang, X.-D.; Wang, T.-H.; Yan, W.-M. Electrocoalescence Behavior of Two Identical Droplets with Various Droplet Radii. *Appl. Therm. Eng.* **2017**, *111*, 1464-1469.

(44) He, X.; Zhang, B.-X.; Wang, S.-L.; Wang, Y.-F.; Yang, Y.-R.; Wang, X.-D.; Lee, D.-J. Electrocoalescence of Two Charged Nanodroplets under Different Types of External Electric Fields. *J. Mol. Liq.* **2021**, *341*, 117417.

(45) Dong, H.; Liu, Y.; Zhou, Y.; Liu, T.; Li, M.; Yang, Z. Mechanism Investigation of Coalescence Behaviors of Conducting Droplets by Molecular Dynamics Simulations. *Colloids and Surfaces A: Physicochemical and Engineering Aspects* **2019**, *570*, 55-62.

(46) Zhou, Y.; Dong, H.; Liu, Y.-H.; Yang, Z.-J.; Liu, T.; Li, M. Molecular Dynamics Simulations of the Electrocoalescence Behaviors of Two Unequally Sized Conducting Droplets. *Langmuir* **2019**, *35* (20), 6578-6584.

(47) Li, S.; Yuan, S.; Zhang, Y.; Guo, H.; Liu, S.; Wang, D.; Wang, Y. Molecular Dynamics Study on the Demulsification Mechanism of Water-in-Oil Emulsion with Sds Surfactant under a Dc Electric Field. *Langmuir* **2022**, *38* (41), 12717–12730.

(48) Li, N.; Sun, Z.; Pang, Y.; Qi, Z.; Liu, W.; Li, W.; Sun, M.; Li, B.; Wang, Z. Microscopic Mechanism for Electrocoalescence of Water Droplets in Water-in-Oil Emulsions Containing Surfactant: A Molecular Dynamics Study. *Sep. Purif. Technol.* **2022**, *289*, 120756.

(49) Li, N.; Sun, Z.; Fan, Y.; Liu, W.; Guo, Y.; Li, B.; Wang, Z. Understanding the Breakup Mechanism of a Droplet under a Dc Electric Field with Molecular Dynamics Simulations and Weak Interaction Analysis. *J. Mol. Liq.* **2021**, *321*, 114475.

(50) Li, N.; Sun, Z.; Liu, W.; Wei, L.; Li, B.; Qi, Z.; Wang, Z. Effect of Electric Field Strength on Deformation and Breakup Behaviors of Droplet in Oil Phase: A Molecular Dynamics Study. *J. Mol. Liq.* **2021**, *333*, 115995.

(51) Li, N.; Sun, Z.; Sun, J.; Liu, W.; Wei, L.; Li, T.; Li, B.; Wang, Z. Deformation and Breakup Mechanism of Water Droplet in Acidic Crude Oil Emulsion under Uniform Electric Field: A Molecular Dynamics Study. *Colloids and Surfaces A: Physicochemical and Engineering Aspects* **2022**, *632*, 127746.

(52) Moradi, M.; Alvarado, V.; Huzurbazar, S. Effect of Salinity on Water-in-Crude Oil Emulsion: Evaluation through Drop-Size Distribution Proxy. *Energy Fuels* **2011**, *25* (1), 260-268.

(53) Morrow, N.; Buckley, J. Improved Oil Recovery by Low-Salinity Waterflooding. *Journal of petroleum Technology* **2011**, *63* (05), 106-112.

(54) Sheng, J. J. Critical Review of Low-Salinity Waterflooding. *Journal of Petroleum Science and Engineering* **2014**, *120*, 216-224.

(55) Katende, A.; Sagala, F. A Critical Review of Low Salinity Water Flooding: Mechanism, Laboratory and Field Application. *J. Mol. Liq.* **2019**, *278*, 627-649.

(56) Chávez-Miyauch, T. E.; Lu, Y.; Firoozabadi, A. Low Salinity Water Injection in Berea Sandstone: Effect of Wettability, Interface Elasticity, and Acid and Base Functionalities. *Fuel* **2020**, *263*, 116572.

(57) Caleman, C.; Van Der Spoel, D. Picosecond Melting of Ice by an Infrared Laser Pulse: A Simulation Study. *Angewandte Chemie International Edition* **2008**, *47* (8), 1417-1420.

(58) Wang, J.; van der Tuuk Opedal, N.; Lu, Q.; Xu, Z.; Zeng, H.; Sjoblom, J. Probing Molecular Interactions of an Asphaltene Model Compound in Organic Solvents Using a Surface Forces Apparatus (Sfa). *Energy Fuels* **2012**, *26* (5), 2591-2599.

(59) Wang, J.; Lu, Q.; Harbottle, D.; Sjoblom, J.; Xu, Z.; Zeng, H. Molecular Interactions of a Polyaromatic Surfactant C5pe in Aqueous Solutions Studied by a Surface Forces Apparatus. *J. Phys. Chem. B* **2012**, *116* (36), 11187-11196.

(60) Yang, F.; Tchoukov, P.; Qiao, P.; Ma, X.; Pensini, E.; Dabros, T.; Czarnecki, J.; Xu, Z. Studying Demulsification Mechanisms of Water-in-Crude Oil Emulsions Using a Modified Thin Liquid Film Technique. *Colloids and Surfaces A: Physicochemical and Engineering Aspects* **2018**, *540*, 215-223.

(61) Xiong, Y.; Cao, T.; Chen, Q.; Li, Z.; Yang, Y.; Xu, S.; Yuan, S.; Sjoblom, J.; Xu, Z. Adsorption of a Polyaromatic Compound on Silica Surfaces from Organic Solvents Studied by Molecular Dynamics Simulation and Afm Imaging. *J. Phys. Chem. C* **2017**, *121* (9), 5020-5028.

(62) Martínez, L.; Andrade, R.; Birgin, E. G.; Martínez, J. M. Packmol: A Package for Building Initial Configurations for Molecular Dynamics Simulations. *J. Comput. Chem.* **2009**, *30* (13), 2157-2164.

(63) Berendsen, H. J.; van der Spoel, D.; van Drunen, R. Gromacs: A Message-Passing Parallel Molecular Dynamics Implementation. *Comput. Phys. Commun.* **1995**, *91* (1-3), 43-56.

(64) Van Der Spoel, D.; Lindahl, E.; Hess, B.; Groenhof, G.; Mark, A. E.; Berendsen, H. J. Gromacs: Fast, Flexible, and Free. *J. Comput. Chem.* **2005**, *26* (16), 1701-1718.

(65) Jorgensen, W. L.; Maxwell, D. S.; Tirado-Rives, J. Development and Testing of the Opls All-Atom Force Field on Conformational Energetics and Properties of Organic Liquids. *J. Am. Chem. Soc.* **1996**, *118* (45), 11225-11236.

(66) Abascal, J. L.; Vega, C. A General Purpose Model for the Condensed Phases of Water: Tip4p/2005. *J. Chem. Phys.* **2005**, *123* (23), 234505.

(67) González, M. A.; Abascal, J. L. The Shear Viscosity of Rigid Water Models. *J. Chem. Phys.* **2010**, *132* (9), 096101.

(68) Vega, C.; Abascal, J.; Nezbeda, I. Vapor-Liquid Equilibria from the Triple Point up to the Critical Point for the New Generation of Tip4p-Like Models: Tip4p/Ew, Tip4p/2005, and Tip4p/Ice. *J. Chem. Phys.* **2006**, *125* (3), 034503.

(69) Guevara-Carrion, G.; Vrabec, J.; Hasse, H. Prediction of Self-Diffusion Coefficient and Shear Viscosity of Water and Its Binary Mixtures with Methanol and Ethanol by Molecular Simulation. *J. Chem. Phys.* **2011**, *134* (7), 074508.

(70) Tsimpanogiannis, I. N.; Moultos, O. A.; Franco, L. F.; Spera, M. B. d. M.; Erdős, M.; Economou, I. G. Self-Diffusion Coefficient of Bulk and Confined Water: A Critical Review of Classical Molecular Simulation Studies. *Molecular Simulation* **2019**, *45* (4-5), 425-453.

(71) Zeron, I.; Abascal, J.; Vega, C. A Force Field of Li+, Na+, K+, Mg2+, Ca2+, Cl−, and So 4 2− in Aqueous Solution Based on the Tip4p/2005 Water Model and Scaled Charges for the Ions. *J. Chem. Phys.* **2019**, *151* (13), 134504.

(72) Panagiotopoulos, A. Z. Simulations of Activities, Solubilities, Transport Properties, and Nucleation Rates for Aqueous Electrolyte Solutions. *J. Chem. Phys.* **2020**, *153* (1), 010903.

(73) Blazquez, S.; Zeron, I.; Conde, M.; Abascal, J.; Vega, C. Scaled Charges at Work: Salting out and Interfacial Tension of Methane with Electrolyte Solutions from Computer Simulations. *Fluid Phase Equilib.* **2020**, *513*, 112548.

(74) Dodda, L. S.; Cabeza de Vaca, I.; Tirado-Rives, J.; Jorgensen, W. L. Ligpargen Web Server: An Automatic Opls-Aa Parameter Generator for Organic Ligands. *Nucleic Acids Res.* **2017**, *45* (W1), W331-W336.

(75) Dodda, L. S.; Vilseck, J. Z.; Tirado-Rives, J.; Jorgensen, W. L. 1.14* Cm1a-Lbcc: Localized Bond-Charge Corrected Cm1a Charges for Condensed-Phase Simulations. *J. Phys. Chem. B* **2017**, *121* (15), 3864-3870.

(76) Miyamoto, S.; Kollman, P. A. Settle: An Analytical Version of the Shake and Rattle Algorithm for Rigid Water Models. *J. Comput. Chem.* **1992**, *13* (8), 952-962.

(77) Hess, B. P-Lincs: A Parallel Linear Constraint Solver for Molecular Simulation. *Journal of chemical theory and computation* **2008**, *4* (1), 116-122.

(78) Bussi, G.; Donadio, D.; Parrinello, M. Canonical Sampling through Velocity Rescaling. *J. Chem. Phys.* **2007**, *126* (1), 014101.

(79) Allen, M. P.; Tildesley, D. J., *Computer Simulation of Liquids*; Oxford university press, 2017.

(80) Essmann, U.; Perera, L.; Berkowitz, M. L.; Darden, T.; Lee, H.; Pedersen, L. G. A Smooth Particle Mesh Ewald Method. *J. Chem. Phys.* **1995**, *103* (19), 8577-8593.

(81) Lv, G.; Gao, F.; Liu, G.; Yuan, S. The Properties of Asphaltene at the Oil-Water Interface: A Molecular Dynamics Simulation. *Colloids and Surfaces A: Physicochemical and Engineering Aspects* **2017**, *515*, 34-40.

(82) Gao, F.; Xu, Z.; Liu, G.; Yuan, S. Molecular Dynamics Simulation: The Behavior of Asphaltene in Crude Oil and at the Oil/Water Interface. *Energy Fuels* **2014**, *28* (12), 7368-7376.

(83) Hub, J. S.; De Groot, B. L.; Van Der Spoel, D. G_Wham a Free Weighted Histogram Analysis Implementation Including Robust Error and Autocorrelation Estimates. *Journal of chemical theory and computation* **2010**, *6* (12), 3713-3720.